



# CO<sub>2</sub> adsorption in biochars obtained from soursop (*Annona muricata*) seeds by chemical activation with metallic salts

Jhoan M. Camargo López<sup>1,2</sup> · José J. Martínez<sup>1</sup> · María H. Brijaldo<sup>2</sup> · Sergio Acevedo<sup>3,4</sup>

Received: 14 June 2024 / Revised: 27 July 2024 / Accepted: 7 August 2024  
© The Author(s) 2024

## Abstract

Environment remediation is one of the primary goals of sustainable development and anthropogenic activities, and the use of fuels in various industrial processes through combustion has led to an increase in CO<sub>2</sub> as well as big damage to the atmosphere by the greenhouse effect. Biochar has been used for the capture of carbon dioxide due to its high surface area. In this study, we obtained biochar from soursop seeds. The materials were synthesized by pyrolysis of precursor materials and chemical activation with chlorides of Ca and Mg at a concentration of 5% w/v. The effect of the defatting process of the soursop seeds on the obtained carbon was also researched. The absorbed solids were characterized through thermogravimetric analysis, X-ray diffraction, and CO<sub>2</sub> adsorption, followed by infrared spectroscopy, N<sub>2</sub>-physisorption, CO<sub>2</sub>-physisorption, CO<sub>2</sub>, XPS, DRIFTS and TPD of NH<sub>3</sub>. The type of activating agent and pretreatment conditions used were more favorable than the defatted process at obtaining carbons with N<sub>2</sub> surface areas between 26 and 220 m<sup>2</sup>g<sup>-1</sup>. The biochars were analyzed by CO<sub>2</sub> surface area to describe the microporous framework, and the solid with the best CO<sub>2</sub> surface area was the one with the highest CO<sub>2</sub> adsorption. According to the statistical analyses conducted, the evaluated models Langmuir, Freundlich, and Redlich-Peterson presented good fits to the experimental data. However, the Redlich-Peterson model showed the lowest values for the residual variance, which were of the order of 0.001 or less in all cases based on the CO<sub>2</sub> adsorption isotherms on the studied activated carbons. However, the carbons obtained by defatting showed favorable hydrophilic behavior along with adsorption capacities in the bioremediation process and affinity towards of this GHG.

**Keywords** Biochar · Soursop seeds · Environment remediation · Chemical activation · Carbon dioxide

## 1 Introduction

The carbon footprint is related to the amount of greenhouse gases produced by anthropogenic activities and emitted by a country dependent on economic growth and currently calculated in tons of CO<sub>2</sub> [1]. In Colombia, the carbon footprint does not exceed 4 tons per year, however, an increase

of 1.45 to 1.53 tons per capita between 2020 and 2011 [2] indicates a minor environmental efficiency for this country. Some efforts to decrease the carbon footprint have been made through the development of adsorbent materials. Thus, an economically and environmentally viable way is to use residual biomass to obtain adsorbent biochar for storage and subsequent use of CO<sub>2</sub>.

Biochar (BC) is generally employed in the adsorption of various contaminants [3], due to its low synthesis costs and less expensive regeneration energies than other adsorbents [4]. Some recent reviews on AC from biomass-based sources for CO<sub>2</sub> capture have shown the current potential and trends in the last few years. Biochar is easily obtained by the carbonization of residual biomass with a high lignocellulose content [5]. Its porous structure can be manipulated by distinct methods, and different chemical functional groups are set up into the surface by various treatments using physical and chemical reagents [6], with the aim of increasing CO<sub>2</sub> affinity. Soursop seeds

✉ Sergio Acevedo  
sergio.acevedo@unad.edu.co

<sup>1</sup> Escuela de Ciencias Químicas, Facultad de Ciencias, Universidad Pedagógica y Tecnológica de Colombia, Tunja, 150003 Boyacá, Colombia

<sup>2</sup> Facultad de Estudios a Distancia, Universidad Pedagógica y Tecnológica de Colombia, 150003 Tunja, Colombia

<sup>3</sup> Escuela de Ciencias Básicas, Universidad Nacional Abierta y a Distancia, 152210 Sogamoso, Colombia

<sup>4</sup> Departamento de Química, Universidad Nacional de Colombia, D.C. 110911 Bogotá, Colombia

are a good precursor of adsorbent materials. This tropical fruit contains 30% of its total weight in seeds, which are considered waste [7]. An alternative to the valorization of these seeds is the production of low-cost animal feed, but it isn't possible because of the high content of antinutritional factors and toxic metabolites [8]. Soursop seeds have the potential to be used as a precursor to produce biochar for CO<sub>2</sub> adsorption.

The method of preparation of biochar from seeds that is most known is pyrolysis, however, the conditions of pyrolysis and the presence of the activating agent are the principal variables that improve the CO<sub>2</sub> adsorption on biochar obtained from biomass [9]. The pyrolysis is carried out using a precursor previously impregnated with a solution of H<sub>3</sub>PO<sub>4</sub>, KOH, NaOH, or ZnCl<sub>2</sub>, which produces carbon with a high surface area and microporous framework [10]. These activating agents are efficient, but the byproducts resulting from washing are too harmful to be discarded. Chemical activation using CaCl<sub>2</sub> or MgCl<sub>2</sub> has been recently explored to obtain mesoporous solids, improving CO<sub>2</sub> adsorption [11]. These salts act as dehydrating agents and serve as pore shaper [12]. CaCl<sub>2</sub> forms symmetric pores after the washing process, and the action of MgCl<sub>2</sub> could be similar. In addition, a high heating ramp rate favours the loss of volatile matter, avoiding blockages in the porous framework and decreasing the superficial groups on the surface of carbon.

Different samples of biochar from soursop seeds were obtained, and it has been tested if the oils in the precursor materials interfere with or contribute to CO<sub>2</sub> adsorption and its interaction with activating agents [13]. So, the synthesis of biochars using seeds with high oil content produces bio-oils in the pyrolytic process. In some cases, these byproducts generate interference in the pore frameworks, which makes the pollutants adsorption difficult. Some authors have performed a defatting process with the final purpose of obtaining a cleaning surface and improving the entry of adsorbate molecules [13]. This process was realized on a part of the seeds before the activated process, expecting to improve the adsorption of CO<sub>2</sub>. Although the defatted process does not improve the surface area, the methodology activation with CaCl<sub>2</sub> produced a homogenous surface with intermedium acid sites, which increased the CO<sub>2</sub> adsorption in these samples. Besides with MgCl<sub>2</sub> activating process improve the surface area without defatting, the acidity of the samples increases too, affecting CO<sub>2</sub> adsorption. This precursor is chemically activated with dehydrating agents of low use in the literature regarding the production of this type of adsorbents generating contribution and innovation in the state of the art, after its preparation and characterization, the CO<sub>2</sub> adsorption capacity was evaluated with a view to the future of industrial use.

## 2 Materials and methods

### 2.1 Soursop seeds characterization

Bromatological characterization was conducted in triplicate and included the content of ash, moisture, fiber with acid detergent fiber (ADF)—neutral detergent fiber (NDF), ethereal extract, and amount of protein [14]. The analysis of ADF is related to the percentage of cellulose and lignin in the sample, while the analysis of NDF is related to the content of ADF and hemicellulose. Thermogravimetric analysis was performed in equipment Setaram 1600 using a temperature ramp of 5 °C.min<sup>-1</sup> to 1000 °C in an N<sub>2</sub> atmosphere of 20 mLmin<sup>-1</sup>. The soursop seed samples were pulverized and measured in an alumina crucible of 90 μL; a mass of soursop seed and degreased seeds at 39.4 and 31.2 mg, respectively.

The samples of soursop seeds were washed and crushed to a 1:2 ratio of chemical activation, using CaCl<sub>2</sub> and MgCl<sub>2</sub> to activate agents in magnetic stirring for 6 h; the degreased soursop seeds were taken to Soxhelt extraction with n-hexane in a refluxed system for 4 h, and this was activated in the same form and dried for 12 h at 100 °C.

### 2.2 Preparation of the biochar

The biochars were prepared by the pyrolysis method using chemical activation of the soursop (*Annona muricata*) seeds and defatted soursop seeds as precursor materials to obtain biochar (BC), resulting from the treatment and processing of the soursop fruit and being an agroindustrial waste. The soursop seeds were acquired from a fruit pulp factory in the region through manual recollection. These were cleaned with ionic water, posteriorly it was dried at 100 °C and then passed through a granulometric sieve until obtaining a particle size between 4 and 2 mm using mesh number 2 (size 2 mm). A portion of soursop seed was taken to carry out the defatting process, the precursor was weighed and packed in cellulose paper and placed in a refluxed system in hexane for 6 h, following the process described by Prandy, et al. [15]. The extracts were separated by rota-evaporation to recover the solvent; the sample was weighed and dried to 100 °C to eliminate the hexane excess. The reagents used were MgCl<sub>2</sub>, CaCl<sub>2</sub>, from Bioquigen, and hexane (> 98%) from Sigma-Aldrich hydrochloric acid (Sigma-Aldrich, 37%). The carbons were prepared according to described by Acevedo, et al. [16], using a tubular resistor Lindberg Blue M of 1200 °C TF55035A-1 at 700 °C for a period of 2 h (heating ramp of 5 °C for minute) and maintaining a flow of 50 mLmin<sup>-1</sup> of CO<sub>2</sub> and N<sub>2</sub> mixture (high purity gases,

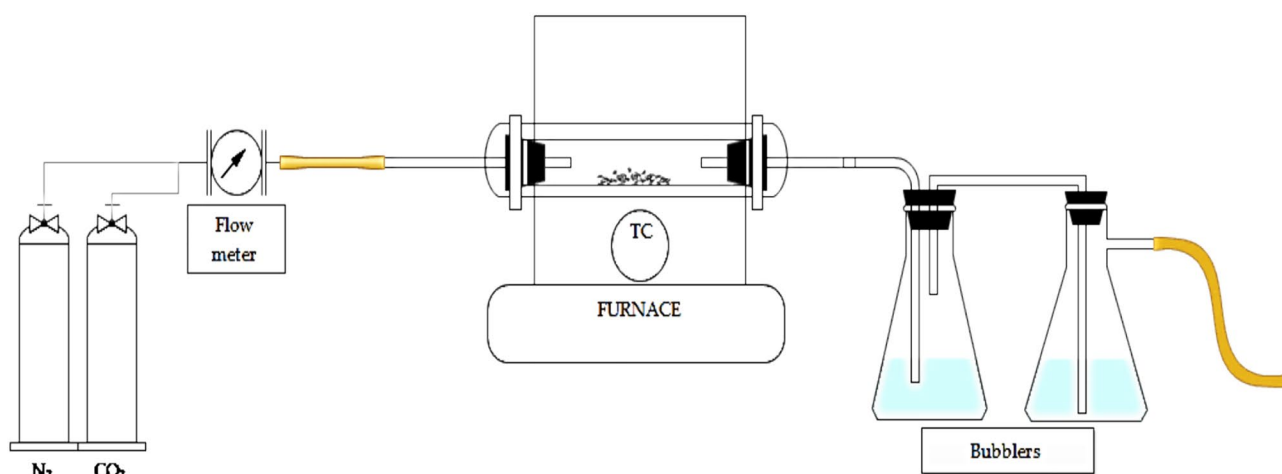


Fig. 1 Scheme of the carbonization system

analytic grade), as can be seen in Fig. 1 [17].  $\text{MgCl}_2$  and  $\text{CaCl}_2$  were used as activating agents at a constant concentration of 5% w/v. The samples of activated carbons were mixed in  $\text{HCl}$  0.01 M to eliminate the activate excess and washed with refluxing in distilled water to a constant pH closer to pH 7.

The adsorbent materials were obtained by pyrolysis of soursop seeds in a tubular oven with a constant flux of  $\text{CO}_2$  and  $\text{N}_2$  mixture out to the bubbler for the retention of bio-oils. The samples were classified by precursor type and activate agent; six samples were obtained that describe the following with their abbreviations:

Soursop seeds	SS
Defatted soursop seeds	DSS
Biochar	BC
Defatted Biochar	DBC
Biochar + $\text{MgCl}_2$	$\text{MgBC}$
Biochar + $\text{CaCl}_2$	$\text{CaBC}$
Degreased Biochar + $\text{MgCl}_2$	$\text{MgDBC}$
Degreased Biochar + $\text{CaCl}_2$	$\text{CaDBC}$

### 2.3 DRX (X-ray diffraction)

The XRDs were obtained by a diffractometer model Mini-Flex with  $\text{CuK}\alpha$  radiation ( $\lambda = 1540 \text{ \AA}$ ). The data were obtained in a range of  $5$  to  $90^\circ$  in  $2\theta$  with an increment of  $0.05^\circ$  as described et al L.M. Esteves [18]. To determine the crystal sizes, the FWH was calculated by the main DRX peaks in the Origin software and using the Debye–Scherrer equation.

### 2.4 FTIR spectra

Infrared spectra were collected by the FTIR-ATR method using an equipment Thermo Scientific model NICOLET iS50 FT-IR spectrometer with a ZnSe window to determine surface groups on the materials. 64 scans were used by each sample [19].

### 2.5 DRIFTS analysis

The same equipment FTIR collected the  $\text{CO}_2$  absorption spectra using a diffuse reflectance accessory with ZnSe. The sample was cooled to  $20^\circ\text{C}$  in an atmosphere of He gas, taking reference spectra of the clean. Then, supply the sample with a flow of  $\text{CO}_2$  ( $30 \text{ mLmin}^{-1}$ ) for 30 min. Finally, the sample was cleaned again with the flow for 10 min, and the last spectrum was collected; this was the absorbed  $\text{CO}_2$  spectrum. To collect the spectra, with a resolution of  $4 \text{ cm}^{-1}$  and 250 scans were used [20].

### 2.6 BET surface area

The values of surface area, diameter, and the pores volume were characterized with a Micromeritics ASAP 2020 analyzer by physisorption of  $\text{N}_2$  at  $-196^\circ\text{C}$ . The samples were previously dried for 12 h in a muffle at  $150^\circ\text{C}$  and degassed employing the vacuum system of the ASAP 2020 equipment for 6 h. The Brunauer–Emmett–Teller (BET) analysis of adsorption–desorption isotherms was employed to calculate the surface area and the pore volume was

calculated from the N<sub>2</sub> desorption curve by the Barrett-Joyner-Halenda (BJH) method [21].

## 2.7 CO<sub>2</sub> adsorption

The carbon dioxide adsorption at 20 °C, the amount of CO<sub>2</sub> physisorbed, and the analysis showed the amount of CO<sub>2</sub> physisorbed in the biochars. The measurements were carried out in the ASAP 2020 Micromeritics analyzer. The samples were degassed under vacuum for 6 h at 150 °C. The weight of the samples was around 100 mg [22]. The measurement of CO<sub>2</sub> adsorption was described by theoretical adsorption isotherm models. Through the study of different models such as Langmuir and Freundlich or models such as Redlich-Peterson, Sips, and Toth, which can describe the interaction biochar- adsorbate in addition to offering characteristics about the nature of the adsorbent and its adsorption mechanism.

## 2.8 NH<sub>3</sub> desorption measurements at the programmed temperature (TPD-NH<sub>3</sub>)

The NH<sub>3</sub> desorption measurements at the programmed temperature (TPD-NH<sub>3</sub>) were carried out in an Auto-ChemII 2920 unit (micromeritics®). Prior to analysis, samples were dried at 150 °C with He (25 mLmin<sup>-1</sup>) for 1 h. The samples were then purged with Heat 400 °C for 30 min and finally cooled to 70 °C to adsorb NH<sub>3</sub> in a 10% NH<sub>3</sub>/He mixture (50 mLmin<sup>-1</sup>) for 30 min. Samples were cleaned with a He flow 25 mLmin<sup>-1</sup> for 1 h to remove excess NH<sub>3</sub>. Then, a constant flow of He from 70 to 900 °C was passed to a heating ramp of 10 °C.min<sup>-1</sup> to obtain the TPD profile [23].

### 2.8.1 X-ray photoelectron spectroscopy (XPS)

XPS spectral analyses were conducted using a Thermo Scientific ESCALAB 250 XI spectrometer. The measurements were performed with a pass energy of 25 eV, an energy step of 0.05 eV, and a time of 50 ms. The pressure within the analysis chamber was maintained around 10<sup>-8</sup> mbar.

## 2.9 Isothermic heats of adsorption

The isosteric heat of adsorption is a thermodynamic property that provides useful information about the adsorbent-adsorbate interaction and the energetic heterogeneity of the adsorption surface. Based on the modified Clausius-Clapeyron equation:

$$q_s t = -RT \left( \frac{\partial \ln(P)}{\partial n} \right)$$

where  $R$  is the gas constant (8.314 JmolK<sup>-1</sup>),  $n$  is the amount of CO<sub>2</sub> adsorbed (molkg<sup>-1</sup>),  $P$  is the pressure of adsorption (kPa) and  $T$  is the temperature in Kelvin (293 K in this case). The isothermal heat corresponds to the energy released in the adsorption process and depends on the temperature and surface coverage. In this study, the isotherms of each sample were used to determine the dependence of the isosteric heat on the adsorbate concentration. The analyses were performed in gas analyzer with prior degassing at 300 °C for 3 h [24].

## 3 Results and discussion

### 3.1 Characterization of soursop seeds

The oil content in the soursop seed was approximately 14.5%, moisture was 7%, protein was 14.2%, and ash was 2.1%. In the seed samples, the TGA mass changes are associated with the loss of moisture or volatile matter in the samples (70–220 °C). Subsequently, the loss of hemicellulose, cellulose, and lignin can be observed up to 900 °C [25], which is depicted in Fig. 2. In the defatted seed samples, temperature changes are more noticeable, particularly in the regions of 70–200 °C and 340–600 °C. The removal of fatty acids embedded in the hemicellulose or cellulose fibers causes thermal degradation to occur more easily. This analysis shows that about 7% can be associated with moisture and volatiles, 55–65% with hemicellulose and cellulose, and approximately 25–30% with lignin. These quantitative results are consistent with those obtained through ADF and NDF. The values of NDF and ADF were 73.4 and 88.4, respectively. This suggests that the resulting carbons could have a higher proportion of disordered porous structures, as has been described by Meng et al. (2021) (Fig. 3).

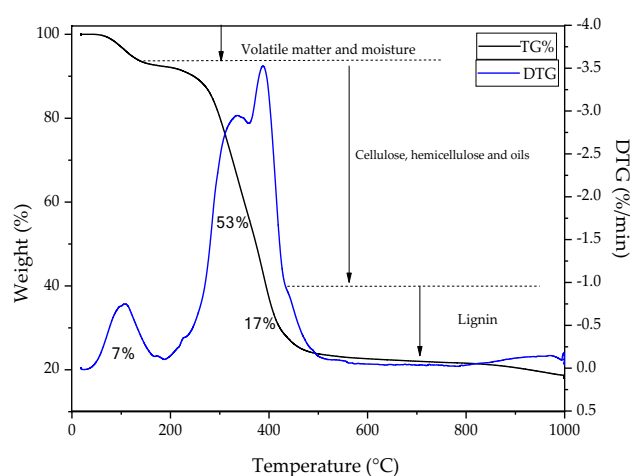
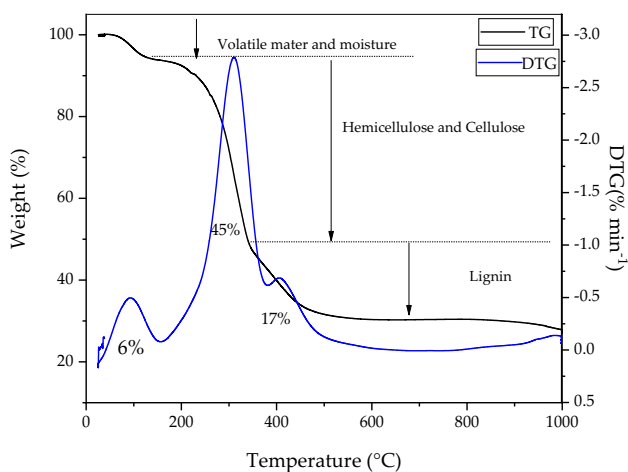


Fig. 2 TGA and DTG curve of soursop seeds (SS)



**Fig. 3** TGA and DTG (percent mass loss) analysis of defatted soursop seeds (DSS)

### 3.2 FTIR spectra

The FTIR spectra of the soursop seeds (Fig. 4a) and defatted soursop seeds (Fig. 4b) showed signals characteristic of biomass organic. These signals correspond to fatty acids, proteins, and the fiber composed of lignin, cellulose, and hemicellulose. Signs of hydrogen bonds stand out between 3200 and 3400  $\text{cm}^{-1}$  and C–H vibration bonds corresponding to 2853 and 2923  $\text{cm}^{-1}$  (only in the precursors); C–O group signals at 1743  $\text{cm}^{-1}$  and other signals below 1600  $\text{cm}^{-1}$  are also highlighted, which are features of deformation of C–O

and C–C bonds vibration characteristic of compounds that contains aromatic rings [26]. After the pyrolytic process, some changes are observed depending on the activating agent and the defatted process. The main bands appeared at 1580  $\text{cm}^{-1}$  (C=O), 1400  $\text{cm}^{-1}$  (C=C), and 1105  $\text{cm}^{-1}$  (C–O–C) [27]. In this case, it is assumed that the pyrolysis process promotes the generation of C=C aromatic skeletal vibrations, as well as changes in C–O–C symmetric and asymmetric vibratory ester groups in cellulose and hemicellulose in the precursor materials, respectively. Comparing the spectra in the presence of an activating agent, the peaks that appear at 850  $\text{cm}^{-1}$  are the same in both samples. According to previous research [28], the signals 1040  $\text{cm}^{-1}$ , and 1400  $\text{cm}^{-1}$  appear in the MgDBC and CaDBC samples; these peaks could be affixed to lengthen of groups (–C=O) and (–C–H), which suggests that the  $\text{MgCl}_2$  or  $\text{CaCl}_2$  in degreased samples may give a hydrophilic biochar.

### 3.3 X-Ray diffractions

The XRD patterns of the biochars obtained are displayed in Fig. 5. The broad peak at 25° is due to the amorphous structure. In the samples, CaBC and CaDBC appear to have a peak at 30° related to CaO with a crystal size of 20 nm and 26 nm, respectively. For MgBC and MgDBC, the peak of MgO appears at 42.6°, and similarly, the crystal size crystal of MgO increases in the defatted sample, reaching 3 nm for MgBC and 16 nm for MgDBC. This increase in the crystal size of CaO or MgO in the degreased samples could be explained by the poor interaction of the salts on the

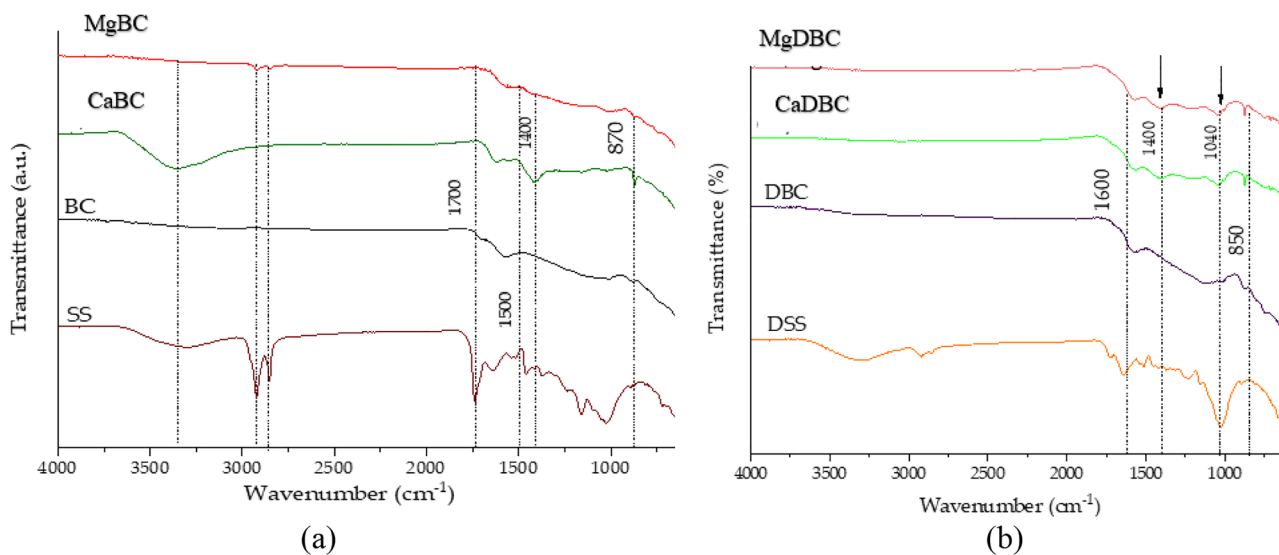


**Fig. 4** FTIR spectra: **a** FTIR biochars analysis activated with metal salts; **b** FTIR analysis of defatted biochars, where SS is the sample of soursop seeds, DSS is the sample of defatted soursop seeds, BC and DBC are biochars of soursop seeds and defatted soursop seeds,

respectively; MgBC and CaBC are biochars activated with metallic salts; and finally, MgDBC and CaDBC are the biochars activate of defatted soursop seeds



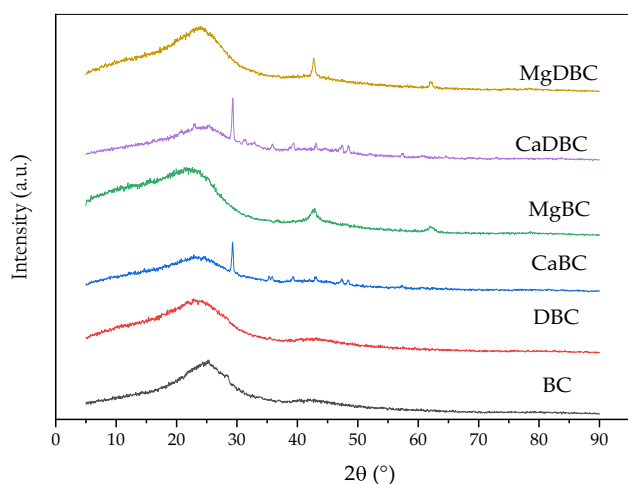


Fig. 5 XRD spectra of biochars

lignocellulosic surface. Besides, the amorphous structure is favored using  $\text{MgCl}_2$  [29].

### 3.4 BET analysis

The BET surface was studied by  $\text{N}_2$  analysis at  $-196^\circ\text{C}$ . A decrease into the surface area ( $S_{\text{BET}}$ ) was showed in the samples treated with  $\text{CaCl}_2$ . Besides, the defatting process and the incorporation of  $\text{CaCl}_2$  do not improve the surface area. However, the addition of  $\text{MgCl}_2$  showed unexpected results. An increase in the  $S_{\text{BET}}$  was observed for MgBC, but the defatting decreases substantially the SBET for MgDBC due to decreases in the volume of the pore, maintaining a similar pore size. The BET area shows a mesoporosity in the material which is useful for the process of agile  $\text{CO}_2$  kinetics within the active sites of the micropores for its adsorption process. It is also shown that the activation temperature is an important factor in the formation and distribution of the porosity obtained in these materials. The results obtained are similar to other studies in which chemical activation was carried out with metallic salts [4, 17] and obtaining

Table 1 Results of  $\text{N}_2$  surface area analysis

Biochar	SBET Area* ( $\text{m}^2\text{g}^{-1}$ )	Poro size (nm)	Vpore ( $\text{cm}^3\text{g}^{-1}$ )	Adsorption isosteric heat (Qst) ( $\text{kJmol}^{-1}$ )
BC	110	4.7	0.12	9.4
DBC	59	6.9	0.10	8.0
MgBC	221	6.1	0.30	8.3
CaBC	85	8.1	0.17	6.9
MgDBC	26	8.1	0.05	11.0
CaDBC	86	4.6	0.10	8.6

\*Corroborated value within the optimal range  $P/P^0$

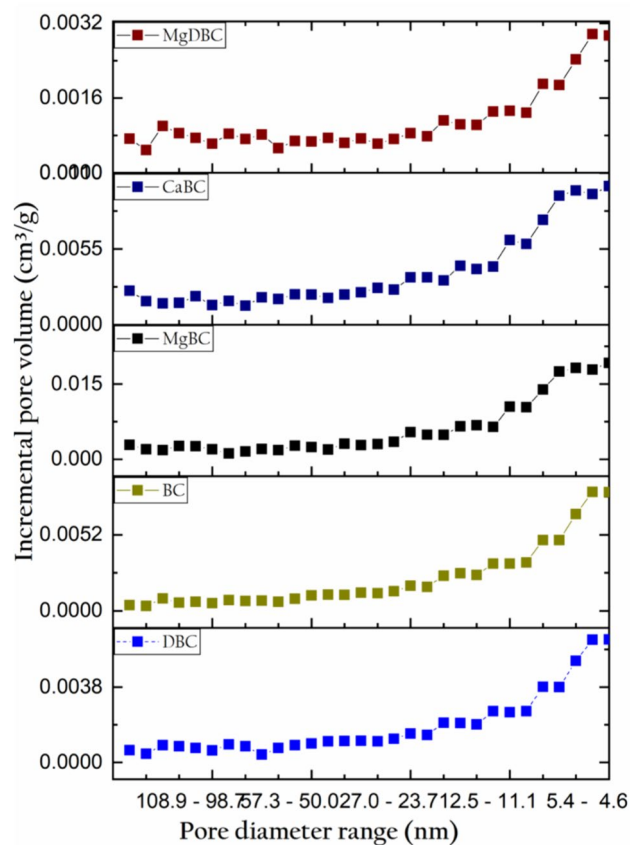


Fig. 6 Incremental pore-size distribution curves of biochars

materials with possible viability in the adsorption process (Table 1).

Figure 6 shows the pore size distribution graphs of the biochars obtained, showing the increase in the pore diameter of all solids with respect to the increase in the total pore volume; this increase is notably observed in the production of narrow and wide mesopores  $< 50$  nm, this is important given that having wider mesopores the speed of access of  $\text{CO}_2$  to the interior of the active sites of the micropores is more favorable.

### 3.5 $\text{CO}_2$ adsorption

In the Fig. 7 it observed the isotherms of  $\text{CO}_2$  adsorption, where the quantity of stored  $\text{CO}_2$  in the biochars was similar, considering that the surface area of the samples was different. It is emphasized that the  $\text{N}_2$  analysis could give erroneous results due to the fact that cryogenic  $\text{N}_2$  cannot be accessed in some micropores [30]. The isotherms are characteristic of type I behavior, which is observed in microporous materials. Although  $\text{CO}_2$  adsorption isn't a usual method for surface area, according to the isotherms obtained (Langmuir shape) of this biochar, most of the pores are in the narrow frame. The quantity of adsorbed  $\text{CO}_2$  increases with

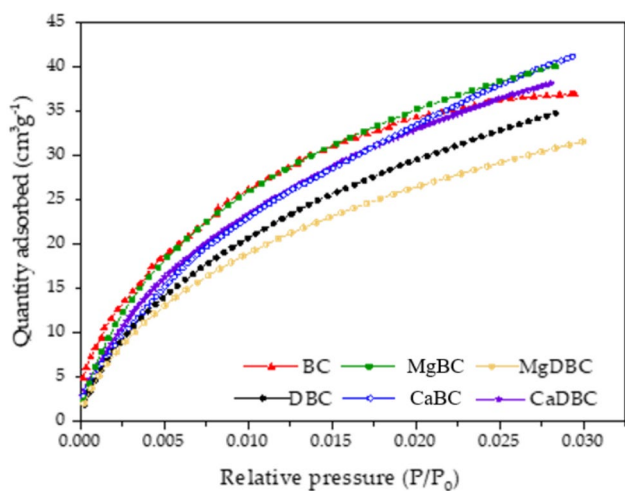


Fig. 7 CO<sub>2</sub> adsorption isotherm of biochars

Table 2 Freundlich and Langmuir models constants and variance data

Adsorption models	Constants	Variance of residuals (reduced chesecure)
<i>BC</i>		
Langmuir	nm(mmolg <sup>-1</sup> )	44.7331
	KL(bar <sup>-1</sup> )	81.7128
Freundlich	Kf(mmolg <sup>-1</sup> )	69.4846
	l/n	0.51598
<i>DBC</i>		
Langmuir	nm(mmolg <sup>-1</sup> )	49.6402
	KL(bar <sup>-1</sup> )	67.9341
Freundlich	Kf(mmolg <sup>-1</sup> )	72.9061
	l/n	0.05349956
<i>CaBC</i>		
Langmuir	nm(mmolg <sup>-1</sup> )	62.2777
	KL(bar <sup>-1</sup> )	50.90756
Freundlich	Kf(mmolg <sup>-1</sup> )	98.6397
	l/n	0.0596728
<i>CaDBC</i>		
Langmuir	nm(mmolg <sup>-1</sup> )	52.5426
	KL(bar <sup>-1</sup> )	78.4297
Freundlich	Kf(mmolg <sup>-1</sup> )	82.8279
	l/n	0.0564639
<i>MgBC</i>		
Langmuir	nm(mmolg <sup>-1</sup> )	52.1674
	KL(bar <sup>-1</sup> )	94.4995
Freundlich	Kf(mmolg <sup>-1</sup> )	78.4443
	l/n	0.0479149
<i>MgDBC</i>		
Langmuir	nm(mmolg <sup>-1</sup> )	43.1575
	KL(bar <sup>-1</sup> )	79.1675
Freundlich	Kf(mmolg <sup>-1</sup> )	66.1917
	l/n	0.0519659

Table 3 Non-linear analysis of Redlich, Toth and Sips models and variance values

Adsorption models	Constants	Variance of residuals (reduced chesecure)
<i>BC</i>		
Redlich-Peterson	K <sub>RP</sub>	8323.71
	A <sub>RP</sub> (bar <sup>-1</sup> )	63.6065
	g	0.646191
Toth	KT(mmolg <sup>-1</sup> )	6368.2
	α <sub>RP</sub> (bar <sup>-1</sup> )	2.28672
	l/t	0.49438
Sips	b(bar <sup>-1</sup> )	44.7357
	nm	5.0553
	1/ns	0.0619503
<i>DBC</i>		
Redlich-Peterson	K <sub>RP</sub>	6945.41
	ARP(bar <sup>-1</sup> )	46.9569
	g	0.634203
Toth	KT(mmolg <sup>-1</sup> )	737.763
	α <sub>RP</sub> (bar <sup>-1</sup> )	0.0147207
	l/t	0.0672859
Sips	b(bar <sup>-1</sup> )	49.6415
	nm	- 20.9106
	1/ns	- 0.307825
<i>CaBC</i>		
Redlich-Peterson	K <sub>RP</sub>	12,113.2
	A <sub>RP</sub> (bar <sup>-1</sup> )	49.6595
	g	0.529836
Toth	KT(mmolg <sup>-1</sup> )	61.4104
	α <sub>RP</sub> (bar <sup>-1</sup> )	0.0167484
	l/t	1.01414
Sips	b(bar <sup>-1</sup> )	62.2809
	nm	61.4062
	1/ns	1.02852
<i>CaDBC</i>		
Redlich-Peterson	K <sub>RP</sub>	1555.41
	A <sub>RP</sub> (bar <sup>-1</sup> )	0.00327877
	g	3.07783
Toth	KT(mmolg <sup>-1</sup> )	7.2346
	α <sub>RP</sub> (bar <sup>-1</sup> )	0.0127506
	l/t	7.26276
Sips	b(bar-1)	- 8948.33
	nm	41.49
	1/ns	- 239.717
<i>MgBC</i>		
Redlich-Peterson	K <sub>RP</sub>	8587.19
	A <sub>RP</sub> (bar <sup>-1</sup> )	69.5857
	g	0.724438
Toth	KT(mmolg <sup>-1</sup> )	132.616
	α <sub>RP</sub> (bar <sup>-1</sup> )	0.0105824
	l/t	0.393376
Sips	b(bar <sup>-1</sup> )	52.1683
	nm	0.0182518
	1/ns	0.000193147
<i>MgDBC</i>		
Redlich-Peterson	K <sub>RP</sub>	6508.18
	A <sub>RP</sub> (bar <sup>-1</sup> )	55.8978
	g	0.675408

**Table 3** (continued)

Adsorption models	Constants	Variance of residuals (reduced chesecquare)	
Toth	KT(mm <sub>ol</sub> g <sup>-1</sup> )	604.874	0.38882
	α <sub>RP</sub> (bar <sup>-1</sup> )	0.0126315	
	l/t	0.0669239	
Sips	b(bar <sup>-1</sup> )	43.1594	0.38882
	nm	0.0342075	
	l/ns	0.000432134	

the pressure, which it can be observed that the biochar has the highest adsorption of CO<sub>2</sub> without activating agents. In fact, these isotherms don't show inflections that mean that the mesopores are clogged by the oils not volatilized in the heating ramp. The fitting data are described in the Tables 2 and 3, using Langmuir, Freundlich, Redlich-Peterson, Toth, and Sips models. These models give an account of how the adsorbate interacts with the biochar and explain how the mechanism of CO<sub>2</sub> adsorption works. The Langmuir model has the major fit with the experimental data obtained for defatted biochar (DBC) and defatted biochar with CaCl<sub>2</sub>, suggesting that this process generates a homogeneous surface on the biochars. On the other hand, other biochars fit the Redlich-Peterson model by supposing that the materials have roughness, and the surface properties are heterogeneous. Consequently, the type of activating agent modifies the surface of the biochar [31].

The evaluation of two- and three-parameter adsorption models and their equilibrium isotherm data allow us to accurately define the surface properties, adsorption mechanisms, and affinity of adsorbents [32]. Therefore, from the CO<sub>2</sub> tests carried out on the biochars and their respective data, the Langmuir, Freundlich, Redlich-Peterson, Sips, and Toth models were tested and analyzed the adsorption behavior, considering the variance of these data in the experimental equilibrium isotherms. In this way, the conditions for the design of adsorption systems would be optimized.

#### 4 Langmuir model

This model proposed by Ivan Langmuir [33] It is a first choice due to the form of CO<sub>2</sub> adsorption and is based on the assumption of a microporous structure that provides an adsorption process at specific homogeneous points on the biochar surface in addition to a monolayer of the adsorbate. It focuses on the premise that biochar has a finite adsorbent capacity (at equilibrium), where the saturation point is achieved without allowing further adsorption. This Langmuir model is plotted to adapt the amount adsorbed in the following equation as described by G. Crini et al. (2007).

$$n_e = \frac{n_m b P_e}{1 + b P_e} \quad (1)$$

In this expression,  $n_e$  is the capacity of adsorbed (mmol g<sup>-1</sup>),  $P_e$  is the gas pressure (bar),  $n_m$  is the highest theoretical adsorption (mmol g<sup>-1</sup>) and  $b$  is the Langmuir isotherm constant.

#### 5 Freundlich model

The Freundlich isotherm is other option very frequent and useful theoretical model in CO<sub>2</sub> adsorption to interpret equilibrium adsorption. It is adjusted for adsorption on surfaces where the adsorbent with a heteroatom-rich surface interacts with the adsorbate molecules (heterogeneous surface). It determines the exponential decrease of adsorption energy to the same extent that the sorption centers end. [34, 35].

The Freundlich equation is as follows:

$$n_e = K_f P_e^{(1/n)} \quad (2)$$

#### 6 Redlich-Peterson

The Redlich-Peterson isotherm model is combined with the characteristics of both the Freundlich and the Langmuir without following the monolayer adsorption model [36], which introduced three parameters in the equation. It has a linear pressure dependence in the numerator, the exponential function and the denominator, which represent an equilibrium adsorption over a wide range of pressures. This model can be used to different systems due to its versatility [37]. However, it must be taken into account that when the adsorption approaches low pressure, the ideal Langmuir condition is reached, and if it approaches high pressure, the ideal condition is Freundlich. The nonlinear model for Redlich-Peterson presents itself as follows:

$$n_e = \left( \frac{K_r P_e}{1 + A_r P_e^g} \right) \quad (3)$$

#### 7 Toth model

The Toth model, although it is an empirical equation, is a model that can improve the adjustments but does not take into account the Langmuir isotherm, it efficiently describes heterogeneous adsorption systems that develop in low and high pressure environments [38]. The following equation shows the Toth model in its non-linear form:



$$n_e = \left( \frac{K_r P_e}{(aT + P_e)^{\frac{1}{r}}} \right) \quad (4)$$

## 8 Sips model

The Sips isotherm, like Redlich, is an adjusted form of the Langmuir and Freundlich expressions. In contrast, this model predicts different adsorption systems, limiting of adsorbate adsorption that occurs in the Freundlich and Redlich models. The nonlinear mathematical model of the Sips isotherm is shown below [34]:

$$n_e = \left( \frac{n_m b P_e^{\frac{1}{n}}}{1 + b P_e^{\frac{1}{n}}} \right) \quad (5)$$

The analysis of variance of residuals (reduced chesecquare) was applied in order to calculate the unknown isotherm parameters, and this models with the lowest variance value presented in the experimental data which were examined. The value of variance of residuals is obtained by Gnuplot (5.4 version) by applying the equations of the different models' software, and the model with the best results was chosen.

Furthermore, the values of the rate constants obtained with these models are not related to the structural and chemical parameters of the activated carbon. This shows that the CO<sub>2</sub> adsorption mechanism is not determined by mass transfer or chemisorption or chemical adsorption due to the formation of chemical bonds between the adsorbent and the adsorbate in the surface monolayer. Additionally, in the samples it is observed that the presence of mesoporosity favors the diffusion of the gas towards the micropores, which are the effective sites of CO<sub>2</sub> adsorption [39].

Considering the models used for CO<sub>2</sub> adsorption, the model that presents the best fit in most of the samples is the Redlich-Peterson model, which facilitates a hybrid analysis that combines characteristics of the Langmuir and Freundlich models, making it a more versatile model for describing adsorption on heterogeneous surfaces at different adsorbate concentrations. Statistical simulation suggests that this model more accurately captures adsorption in the prepared activated carbons, showing that these solids present different types of combined surfaces, while the CaDBC sample fit better to the Tohl model as indicated in Table 2, since this model does not take into account the non-line indicating that there is a heterogeneity on the surface of this material.

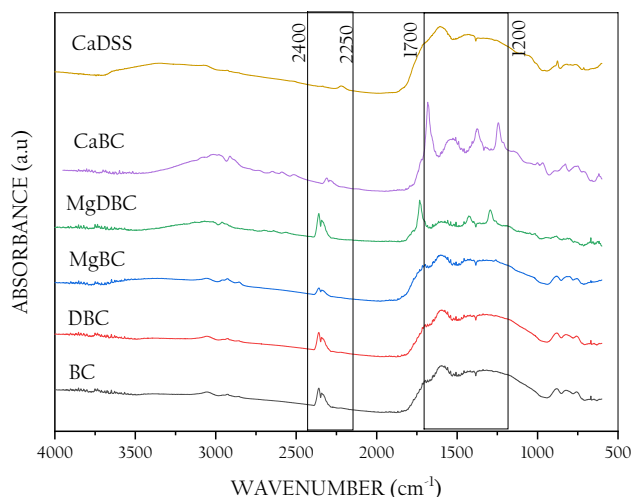


Fig. 8 CO<sub>2</sub> DRIFTS analysis of activated carbons

### 8.1 CO<sub>2</sub> DRIFTS

Drifts under constant CO<sub>2</sub> flow were performed to know the species adsorbed on the surface of solids and are shown in Fig. 8. The chemical groups of the surface O<sub>2</sub> atoms is decisive for the different modes of CO<sub>2</sub> adsorption. Chemisorption of CO<sub>2</sub> reveals both basic and active sites, for example, acid–base pairs if carbonate-like species are built, acidic sites where the CO<sub>2</sub> molecule retains its linear geometry after adsorption [40]. The presence of isolated or low-coordination superficial O<sub>2</sub> anions represents the formation of monodentate carbonates, generally those present in edges. Lewis acid–base pairs manifest as bidentate carbonate (M–O<sub>2</sub> pair site, M is the metal cation Ca or Mg) and bicarbonate production involves surface hydroxyl groups. DRIFTS analysis show that they correspond to CO<sub>2</sub> gas between 2400 and 2200 cm<sup>-1</sup> associated with acidic sites where the carbonic dioxide molecule preserves the linear geometry [40]. The signals found around 1600 cm<sup>-1</sup> correspond to monodentate carbonates.

### 8.2 NH<sub>3</sub> desorption measurements at the programmed temperature (TPD-NH<sub>3</sub>)

In general, the strong acid is classified according to the desorption peaks and the temperature at which they appear, as follows: weak (< 150 °C), medium (150 and 400 °C), and strong (> 400 °C). They can also be correlated with Lewis's acid sites (below 400 °C) and Brønsted acid sites (above 400 °C) [20]. The strong of the acid sites was determined by NH<sub>3</sub> TPD (Fig. 9). Three of the obtained biochars were compared: biochar activated with CaCl<sub>2</sub> (CaBC), biochar activated with MgCl<sub>2</sub> (MgBC), and non-activated biochar (BC). The TPD plots show that the

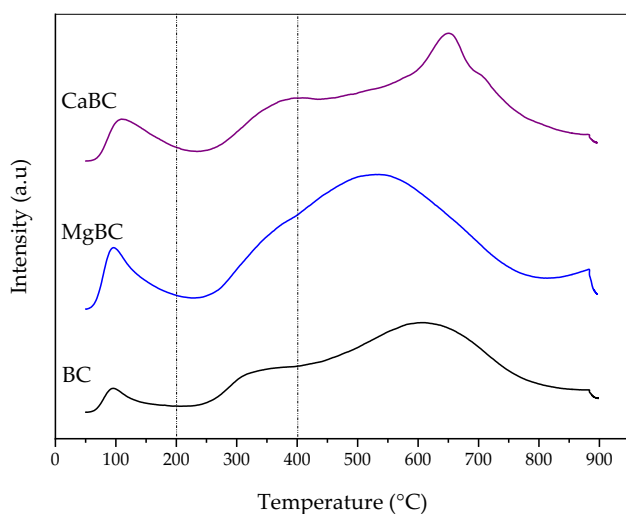


**Fig. 9**  $\text{NH}_3$  TPD profiles for BC, MgBC and CaBC

$\text{MgCl}_2$  activation process increases the acid sites in the biochar, on the other hand, the  $\text{CaCl}_2$  activation process shows that the strong acid sites decrease, i.e., the Brønsted acid sites decrease considerably. Although MgBC has a higher surface area, it does not adsorb more  $\text{CO}_2$  than CaBC due to the interaction on the biochar.

### 8.3 X-ray photoelectron spectroscopy (XPS)

Figure 10 shows the XPS results for the biochars obtained in the study to C 1 s and N 1 s. In the biochars (BC), three distinct peaks are identified, which are generally attributed to contributions from C=C in graphitic carbon (284.6 eV), C–C (285.5 eV), and COOR groups (288.0–289 eV). The relative intensity of the peaks corresponding to C–C hybridisation increases with the incorporation of Mg (MgDBC 3.35%), suggesting a higher presence of defects in the structure during the activation process. In the MgBC samples, this peak increases due to a higher concentration of defective oxygen associated with MgO (which has a smaller particle size) [41, 42]. Additionally, upon activating the biochars with Ca and Mg and assessing the impact of fats, very similar signals for carbon and nitrogen were observed, which is related to the amount of proteins of lignocellulosic precursor. Nitrogen can be present in various forms in biochar, depending on the biomass source and pyrolysis conditions. For biochars from soursop seeds, N1s signals were found at  $\sim 398.0$ – $398.6$  eV. This peak is attributed to nitrogen atoms that are part of pyridine-type aromatic rings. Additionally, a peak was detected at  $\sim 399.8$ – $400.4$  eV, which is associated with nitrogen atoms that are part of pyrrole-type aromatic rings, including nitrogen in pyrrolidine-type structures.

### 8.3.1 FTIR spectra after $\text{CO}_2$ adsorption on biochars

Figure 11 shows the Infrared spectra after  $\text{CO}_2$  adsorption on biochars. The characteristic bands of carbonyl (C=O), hydroxyl (OH), aromatic (C=C) and aliphatic (C–H) groups [26–28] kept similar after  $\text{CO}_2$  adsorption. The above behavior indicates that the  $\text{CO}_2$  adsorption does not noticeably modify the surface of the biochars. The above bands were also observed in the FTIR and DRIFTS of in situ  $\text{CO}_2$  adsorption of the samples observed in Figs. 4 and 8 respectively.

### 8.4 Isosteric heats of adsorption

To calculate the isosteric heat of adsorption of  $\text{CO}_2$ , the modified Clausius Clapeyron equation was used at a constant temperature using the pressure data and the moles of adsorbed  $\text{CO}_2$  obtained in the  $\text{CO}_2$  adsorption isotherm. Table 1 shows the average value of isosteric heat of adsorption of  $\text{CO}_2$  to biochars. The isosteric heat of adsorption was ranged from 8.0 to  $11.0 \text{ kJmol}^{-1}$  and it was still located in the range of physical adsorption ( $< 50 \text{ kJmol}^{-1}$ ). This behavior indicates that no strong chemical bond was formed between  $\text{CO}_2$  and the biochars surface. The sample MgDBC showed the higher  $q_{st}$  value that the other samples, following BC sample, which reveal a strong affinity of the MgDBC and BC to  $\text{CO}_2$  molecule. Likewise, the degreased biochars that were prepared with Ca and Mg activators presented a higher average  $Q_{st}$  value, compared to their corresponding undegreased samples. This possibly indicates that the degreasing process favors the presence of higher energy sites, which causes a greater affinity of  $\text{CO}_2$  and the surface of these samples.

Figure 12 shows the isosteric heat of adsorption of  $\text{CO}_2$  on biochars. In general, the biochars exhibited isosteric heats of  $54 \text{ kJmol}^{-1}$  to  $1.5 \text{ kJmol}^{-1}$ , in the range of 0.1 to  $1 \text{ molkg}^{-1}$   $\text{CO}_2$  adsorption capacity. In all cases, as  $\text{CO}_2$  adsorption increased, isosteric heat decreased as occurs in most biochars. The above behavior is due to that the  $\text{CO}_2$  is adsorbed first in the higher energy adsorption sites, therefore contributing to a higher initial isosteric heat of adsorption.

#### 8.4.1 $\text{CO}_2$ adsorption mechanism

Considering the results obtained from the characterization analyses in this study, a soursop seed biochar with a heterogeneous surface (Fig. 13) could be proposed, which includes micropores and mesopores mostly, determined by  $\text{N}_2$  physisorption, and different functional groups (hydroxyl, carboxyl, carbonyl, etc.) detected by FTIR. The  $\text{CO}_2$  adsorption mechanism on biochar involves several steps, from the diffusion of  $\text{CO}_2$  to its interaction with the biochar surface and the functional groups present. The steps of the process

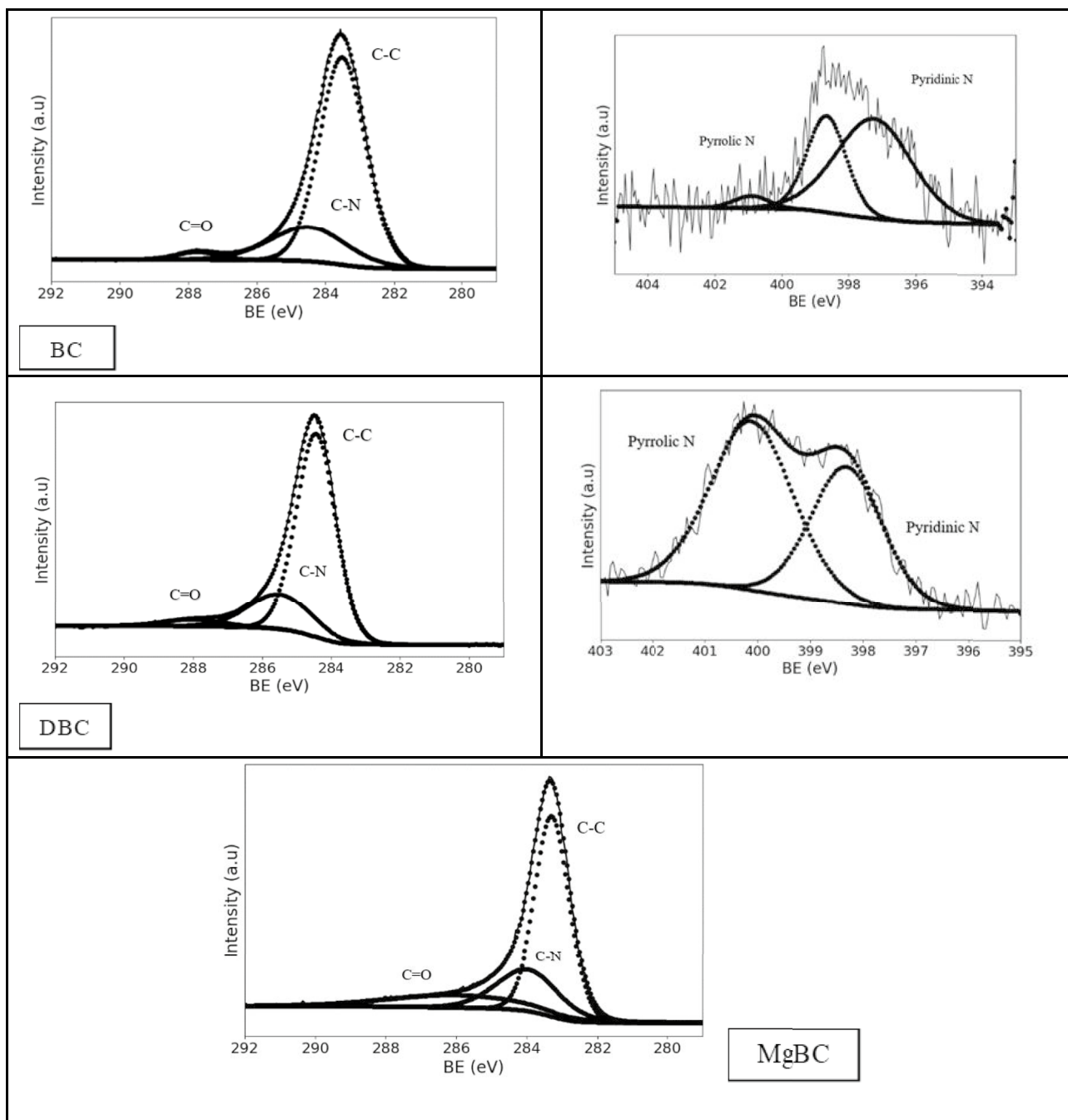


**Fig. 10** XPS analysis of activated carbons. \*N<sub>2</sub> signal was not detected to MgBC

are typical of an adsorption. For this, the CO<sub>2</sub> molecules move from the environment to the biochar surface by diffusion. Then these molecules adhere to the external surface of the biochar possibly through Van der Waals forces, which correspond to a physisorption. In certain cases, CO<sub>2</sub> can form chemical bonds with functional groups on the biochar surface, such as hydroxyl, carboxyl and carbonyl groups and other. Subsequently, CO<sub>2</sub> moves through the larger pores in the biochar structure and penetrates into the micropores,

where it can be adsorbed more effectively due to the stronger interactions in these pores. Then, CO<sub>2</sub> molecules adhere to the inner walls of the pores, through physical interactions, as indicated by the low average isosteric heat values found in the soursop seed biochars and in the presence of reactive functional groups, chemical adsorption can occur within the pores or active sites, which can increase the adsorption capacity of the biochar. The nature of these active sites of the biochar corresponds mostly to surfaces with C=C or

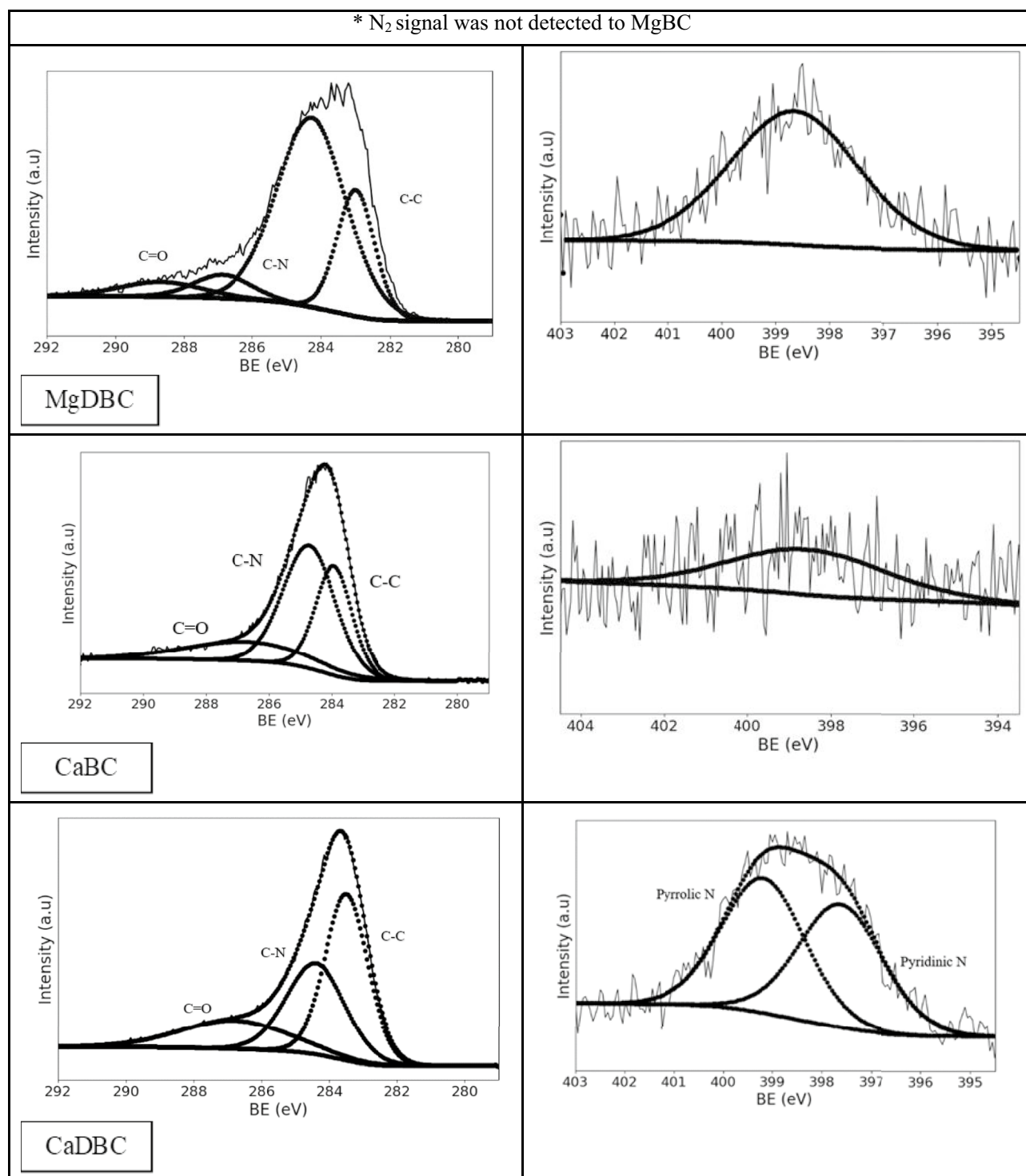
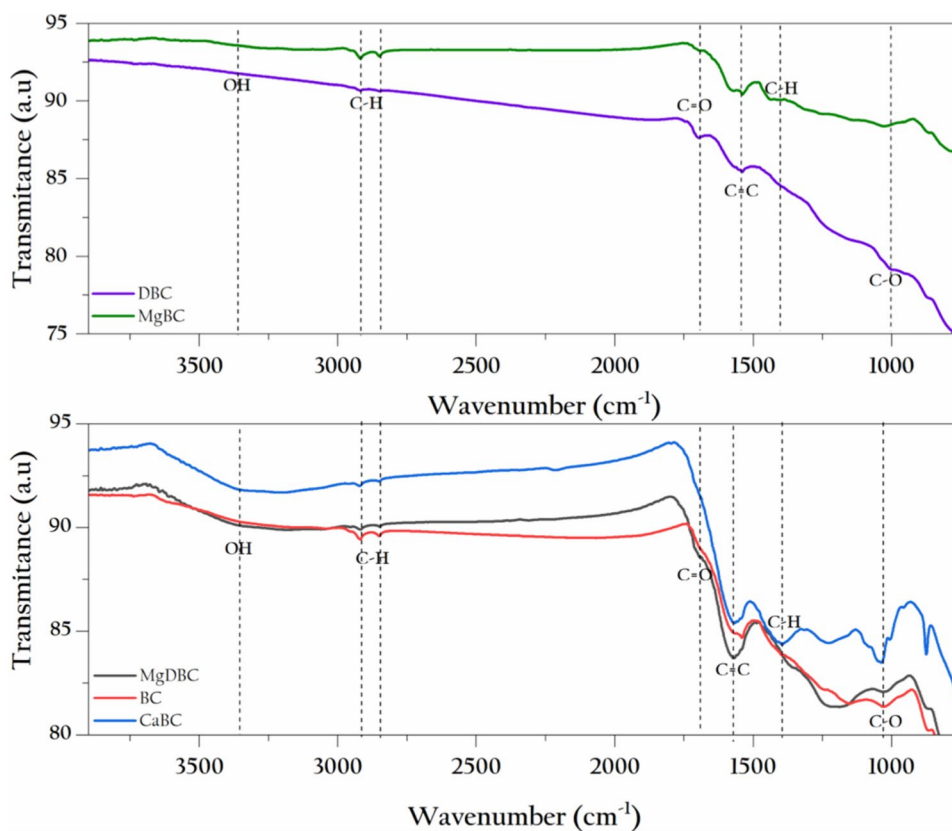


Fig. 10 (continued)

C–C bonds, as indicated by the XPS spectra performed. Finally, a dynamic equilibrium between the adsorption and desorption of CO<sub>2</sub> can be reached. According to the DRIFTS analyses carried out, the CO<sub>2</sub> is adsorbed through carbonate, bicarbonate, and molecular species [43]. According to the

models applied in this study, the Redlich-Peterson model has great prevalence over the others, which confirms that the biochars obtained have a varied (heterogeneous) surface, which means that the surface is not uniform and can have different characteristics at different points.

**Fig. 11** FTIR of biochar samples after CO<sub>2</sub> adsorption



### 9 Conclusions

The process of defatting the soursop seeds does not improve the surface of the biochars, but this, added to the activation process with CaCl<sub>2</sub>, improved the adsorption of CO<sub>2</sub> since the surface of the biochar was heterogeneous. Furthermore, this activation process decreases the acidity of the biochar, allowing for better CO<sub>2</sub> adsorption. In the case of the activation process with MgCl<sub>2</sub>, the surface area increased as did the acidity of the samples, which did not take advantage of CO<sub>2</sub> adsorption.

The biochars prepared in this research obtained surface areas between 26 and 221 m<sup>2</sup>g<sup>-1</sup> and pore volumes 0.05–0.30 cm<sup>3</sup>g<sup>-1</sup>. The CO<sub>2</sub> adsorption capacities are within values of 30–42 cm<sup>3</sup>g<sup>-1</sup> which demonstrate that the micro-mesoporous porous network formed helps the GHG adsorption process given the broad mesoporosity that generates routes of greater accessibility of the adsorbate to the interior of the micropores.

The substituent groups of these biomolecules remain on the surface of the solid after carbonization, favoring the adsorption of CO<sub>2</sub>, especially in the case of solids with reduced surface areas, resulting in similar amounts of CO<sub>2</sub> adsorption as reported in previous research.

The fit of the CO<sub>2</sub> adsorption isotherms to the Langmuir and Redlich models suggests that the biochars have been

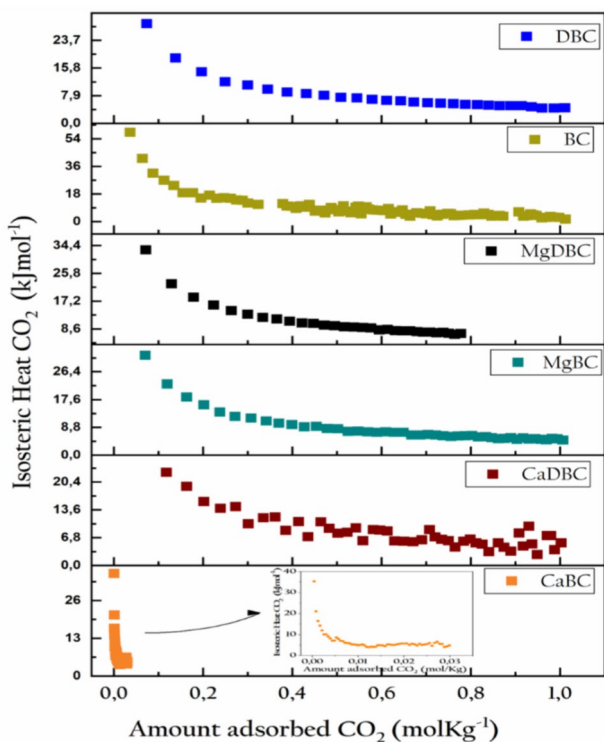
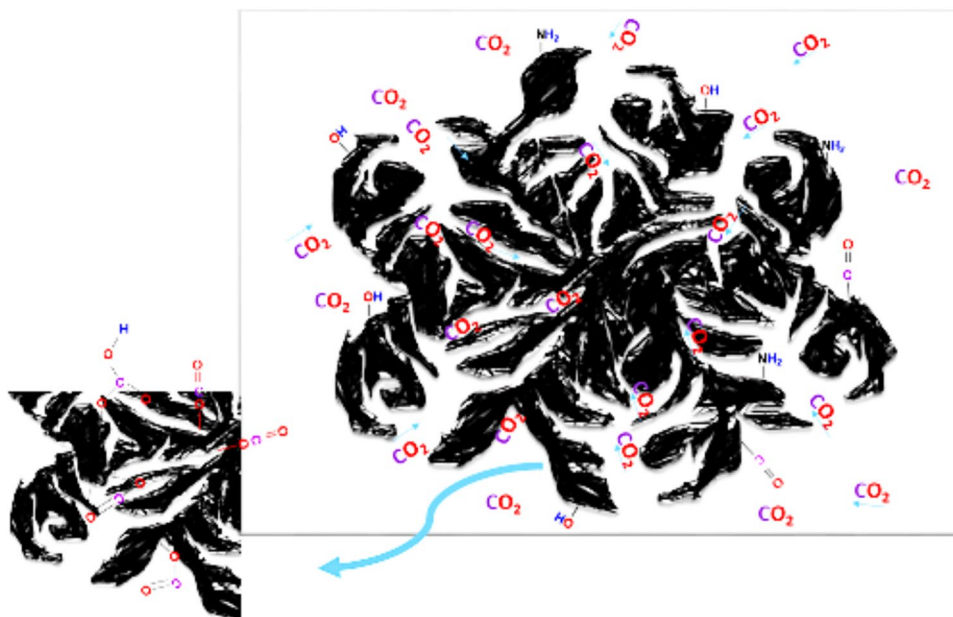


**Fig. 12** Isosteric heat of adsorption of CO<sub>2</sub> on Biochars estimated by the Clausius–Clapeyron equation modified



**Fig. 13** Possible CO<sub>2</sub> adsorption mechanism on Biochars from soursop seed



solid with a mostly mixed surface; biochars such as DBC and CaDBC were materials with a homogeneous surface due to their fit to the Langmuir model.

One way to improve surface area is to increase the heating rate because volatile loss is better than using a slow rate. It was evidenced in the pore size, since the pores were of similar size, but the surface area changed, having different values. This suggests that the porous structure was obstructed by the lack of volatile matter. Regarding the defatting process, an attempt would be made to use a supercritical fluid process to improve the radial pentagon of biochar synthesis.

**Acknowledgements** The authors greatly acknowledge the support provided by the Universidad Pedagógica y Tecnológica de Colombia (VIE-SGI 3433) and Universidad Nacional Abierta y a Distancia (ECBTI), Departamento de Química, Facultad de Ciencias, Universidad Nacional de Colombia and Peslac®.

**Author contributions** Jhoan M. Camargo López: carried out the conceptualization of the research by writing the draft article, he also carried out the bibliographic search and the experiments, obtaining the metadata of the investigation and finally the data analysis. José J. Martínez Z: carried out the verification and analyzed results, together with the review and final edition of the manuscript. María H. Brijaldo Ramírez: carried out the verification and analyzed results, together with the review and final edition of the manuscript. Sergio Acevedo: carried out the verification and analyzed results, together with the review and final edition of the manuscript.

**Funding** Open Access funding provided by Colombia Consortium. The research experimental was funded by the (UPTC) Universidad Pedagógica y Tecnológica de Colombia and the Vicerrectoría de Investigación y Extensión by the project SGI code 3254.

**Data availability** The authors of the present investigation corroborate that the data supporting the findings of this investigation are available

in the article, and additional information may be obtained by sending an email to the corresponding author, upon reasonable request.

## Declarations

**Conflict of interest** The authors declare no competing interests.

**Ethical approval** The authors of this research certify that the presentation is a unique—original work and is not currently under review in any journal or other publication.

**Consent to participate** All the authors described in this work have seen, reviewed and agree with the entire content of the manuscript.

**Consent for publication** All authors agree to submit this manuscript for review and publication in this journal.

**Open Access** This article is licensed under a Creative Commons Attribution 4.0 International License, which permits use, sharing, adaptation, distribution and reproduction in any medium or format, as long as you give appropriate credit to the original author(s) and the source, provide a link to the Creative Commons licence, and indicate if changes were made. The images or other third party material in this article are included in the article's Creative Commons licence, unless indicated otherwise in a credit line to the material. If material is not included in the article's Creative Commons licence and your intended use is not permitted by statutory regulation or exceeds the permitted use, you will need to obtain permission directly from the copyright holder. To view a copy of this licence, visit <http://creativecommons.org/licenses/by/4.0/>.

## References

1. Afrouzi, H.N., Ahmed, J., Siddique, B.M., Khairuddin, N., Hassan, A.: Results in engineering review article a comprehensive review on carbon footprint of regular diet and ways to improving lowered emissions. *Results Eng.* **18**, 101054 (2023). <https://doi.org/10.1016/j.rineng.2023.101054>

2. Su, E.Y., Con, R., Paola, B., Salcedo, C., Rivera, C.V.: Puerta Roja de la Universidad de Sucre—Colombia evaluation of the ecological footprint and its relationship with the biological capacity at the puerta roja campus of the University of Sucre—Colombia. *Rev. Investig. en Gestión Ind. Ambient. Segur. y Salud en el Trab.* (2022). <https://doi.org/10.34893/gisst.v8i1.422>
3. Abuelnoor, N., Alhajaj, A., Khaleel, M., Vega, L.F.: Chemosphere Activated carbons from biomass-based sources for CO<sub>2</sub> capture applications. *Chemosphere* **282**, 131111 (2021). <https://doi.org/10.1016/j.chemosphere.2021.131111>
4. Manyà, J.J., González, B., Azuara, M., Arner, G.: Ultra-microporous adsorbents prepared from vine shoots-derived biochar with high CO<sub>2</sub> uptake and CO<sub>2</sub>/N<sub>2</sub> selectivity. *Chem. Eng. J.* **345**, 631–639 (2018). <https://doi.org/10.1016/j.cej.2018.01.092>
5. Torres, D., Sonia, J., Morales, P., Juan, V., Quintero, C.: “Evaluación de pretratamientos químicos sobre materiales lignocelulósicos chemical pretreatments evaluation on lignocellulosic materials. *Ingeniare. Rev. Chil. Ing.* **25**, 733–743 (2017). <https://doi.org/10.4067/S0718-33052017000400733>
6. Sharma, G., et al.: Activated carbon as superadsorbent and sustainable material for diverse applications. *Adsorpt. Sci. Technol.* (2022). <https://doi.org/10.1155/2022/4184809>
7. Soli, J.A.: Soursop (*Annona muricata* L.) Seeds, therapeutic and possible food potential. Elsevier (2011)
8. Komansilan, A., Abadi, A.L., Yanuwadi, B., Kaligis, D.A.: Isolation and identification of biolarvicide from soursop (*Annona muricata* Linn.) seeds to mosquito (*Aedes aegypti*) larvae. *Int. J. Eng. Technol.* **12**(3), 28–32 (2012)
9. Acevedo, S., Giraldo, L., Moreno-Piraján, J.C.: Kinetic study of CO<sub>2</sub> adsorption of granular-type activated carbons prepared from palm shells. *Environ. Sci. Pollut. Res.* (2023). <https://doi.org/10.1007/s11356-023-26423-5>
10. Jasri, K., Saud, A., Jawad, A.H., Allothman, Z.A., Yousef, T.A., Al Duaij, O.K.: Diamond & related materials mesoporous activated carbon produced from mixed wastes of oil palm frond and palm kernel shell using microwave radiation-assisted K<sub>2</sub>CO<sub>3</sub> activation for methylene blue dye removal : optimization by response surface methodology. *Diam. Relat. Mater.* (2023). <https://doi.org/10.1016/j.diamond.2022.109581>
11. Acevedo, S.: Adsorption of CO<sub>2</sub> onto activated carbons prepared by chemical activation with metallic salts. *Int. J. Chem. Reactor Eng.* **15**, 1–11 (2018). <https://doi.org/10.1515/ijcre-2017-0198>
12. Giraldo, L., Vargas, D.P., Moreno-Piraján, J.C.: Study of CO<sub>2</sub> adsorption on chemically modified activated carbon with nitric acid and ammonium aqueous. *Front. Chem.* (2020). <https://doi.org/10.3389/fchem.2020.543452>
13. Marrakchi, F., Hameed, B.H., Bouaziz, M.: Mesoporous and high-surface-area activated carbon from defatted olive cake by-products of olive mills for the adsorption kinetics and isotherm of methylene blue and acid blue 29. *J. Environ. Chem. Eng.* **8**(5), 104199 (2020). <https://doi.org/10.1016/j.jece.2020.104199>
14. Raffrenato, E., Van Amburgh, M.E.: Technical note : improved methodology for analyses of acid detergent fiber and acid detergent lignin. *J. Dairy Sci.* **94**(7), 3613–3617 (2011). <https://doi.org/10.3168/jds.2010-3701>
15. Prandi, B., Ruales, J., Van Camp, J., Sforza, S., Elst, K.: Valorization of soursop (*Annona muricata*) seeds as alternative oil and protein source using novel de-oiling and protein extraction techniques. *LWT* (2023). <https://doi.org/10.1016/j.lwt.2023.114777>
16. Acevedo Corredor, S.: Preparación y caracterización de carbón activado granular obtenido a partir de cuesco de palma africana (*Elaeis Guineensis*) para la adsorción de CO<sub>2</sub> (2014)
17. Acevedo Corredor, S.: Activación química de cuesco de palma africana (*Elaeis Guineensis*) con soluciones de sales metálicas en la preparación de carbones activados para la adsorción de CO<sub>2</sub> (2019)
18. Esteves, L.M., Brijaldo, M.H., Passos, F.B.: Decomposition of acetic acid for hydrogen production over Pd/Al<sub>2</sub>O<sub>3</sub> and Pd/TiO<sub>2</sub>: influence of metal precursor. *J. Mol. Catal. A Chem.* **422**, 275–288 (2016). <https://doi.org/10.1016/j.molcata.2016.02.001>
19. Castañeda, C., Tzompantzi, F., Gómez, R., Rojas, H.: Enhanced photocatalytic degradation of 4-chlorophenol and 2,4-dichlorophenol on in situ phosphated sol-gel TiO<sub>2</sub>. *J. Chem. Technol. Biotechnol.* **91**(8), 2170–2178 (2016). <https://doi.org/10.1002/jctb.4943>
20. Brijaldo, M.H., Mancipe, S., Rojas, H.A., Viviana, P.L., Araiza, D.G., Díaz, G.: “Effect of boron on the surface properties of nickel supported on hydrotalcite-type mixed oxides in methanol decomposition. *Mol. Catal.* (2020). <https://doi.org/10.1016/j.mcat.2020.111262>
21. Brijaldo, M.H., Rojas, H.A., Martínez, J.J., Passos, F.B.: Effect of support on acetic acid decomposition over palladium catalysts. *J. Catal.* **331**, 63–75 (2015). <https://doi.org/10.1016/j.jcat.2015.08.019>
22. Giraldo, L., Moreno, J.C.: Adsorción de CO<sub>2</sub> en carbón activado con diferente grado de activación. *Afinidad* **67**, 548 (2010). <https://raco.cat/index.php/afinidad/article/view/269277>
23. Rojas, H.A., Martínez, J.J., Brijaldo, M.H., Passos, F.: Producción de alcohol cinamílico a partir de la hidrogenación selectiva de cinamaldehído usando catalizadores de oro soportados en óxidos metálicos. *Rev. la Acad Colomb. Ciencias Exactas Físicas y Nat.* **43**, 539–549 (2019). <https://doi.org/10.18257/racce fyn.852>
24. Balathanigaimani, M.S., Shim, W.G., Lee, J.W., Park, K.H.: Effects of structural and surface energetic heterogeneity properties of novel corn grain-based activated carbons on dye adsorption. *Micropor. Mesopor. Mat.* **118**, 232–238 (2009). <https://doi.org/10.1016/j.micromeso.2008.08.028>
25. Yang, H.: Characteristics of hemicellulose, cellulose and lignin pyrolysis. *Fuel* **86**, 1781–1788 (2007). <https://doi.org/10.1016/j.fuel.2006.12.013>
26. Schroeder, P., do Nascimento, B.P., Romeiro, G.A., Figueiredo, M.K.K., da Cunha Veloso, M.C.: Chemical and physical analysis of the liquid fractions from soursop seed cake obtained using slow pyrolysis conditions. *J. Anal. Appl. Pyrolysis* **124**, 161–174 (2017). <https://doi.org/10.1016/j.jaap.2017.02.010>
27. Hu, Q., Zhang, Z.: Application of Dubinin-Radushkevich isotherm model at the solid/solution interface: a theoretical analysis. *J. Mol. Liq.* **277**, 646–648 (2019). <https://doi.org/10.1016/j.molliq.2019.01.005>
28. Yao, X., Li, L., Li, H., He, S.: A new method for preparing hydrophilic-activated carbon through ester hydrolysis in an alkaline environment. *J. Mater. Sci.* **49**(14), 4807–4815 (2014). <https://doi.org/10.1007/s10853-014-8180-9>
29. Tu, W., Hallett, J.P.: ScienceDirect recent advances in the pre-treatment of lignocellulosic biomass. *Curr. Opin. Green Sustain. Chem.* **20**, 11–17 (2019). <https://doi.org/10.1016/j.cogsc.2019.07.004>
30. Kim, K.C., Yoon, T.U., Bae, Y.S.: Applicability of using CO<sub>2</sub> adsorption isotherms to determine BET surface areas of microporous materials. *Micropor. Mesopor. Mater.* **224**, 294–301 (2016). <https://doi.org/10.1016/j.micromeso.2016.01.003>
31. Abunowara, M., Bustam, M.A., Sufian, S., Eldemerdash, U.: Description of carbon dioxide adsorption and desorption onto Malaysian coals under subcritical condition. *Procedia Eng.* **148**, 600–608 (2016). <https://doi.org/10.1016/j.proeng.2016.06.521>
32. Santhi, T., Manonmani, S., Smitha, T.: Removal of methyl red from aqueous solution by activated carbon prepared from the *Annona squamosa* seed by adsorption. *Chem. Eng. Res. Bull.* **14**(1), 10–18 (2010). <https://doi.org/10.3329/ceerb.v14i1.3767>

33. Langmuir, I.: The adsorption of gases on plane surfaces of glass, mica and platinum. *J. Am. Chem. Soc.* **345**, 1918 (1914). <https://doi.org/10.1021/ja02242a004>
34. Crini, A., Badot, P.: Application of chitosan, a natural aminopolysaccharide, for dye removal from aqueous solutions by adsorption processes using batch studies : a review of recent literature. *Prog. Polym.* **33**, 399–447 (2008). <https://doi.org/10.1016/j.progpolymsci.2007.11.001>
35. Freundlich, H.M.F.: Over the adsorption in solution. *J. Phys. Chem.* **57**, 1100–1107 (1906)
36. Nasr, A.H.M.F., Latifa, A.J.F.: Aminated acrylic fabric waste derived sorbent for Cd (II) Ion removal from aqueous solutions : mechanism, equilibria and kinetics. *J. Polym. Environ.* (2020). <https://doi.org/10.1007/s10924-020-01863-z>
37. Redlich, O., Peterson, D.L.: A useful adsorption isotherm. *J. Phys. Chem.* **63**(6), 1024 (1959)
38. Toth, J.: State equation of the solid-gas interface layers. *Acta Chim. Hung.* **69**, 311–328 (1971)
39. Yu, X.X., Liu, B., Shen, Y.H., Zhang, D.H.: Design and experiment of high-productivity two-stage vacuum pressure swing adsorption process for carbon capturing from dry flue gas. *Chin. J. Chem. Eng.* **43**, 378–391 (2022). <https://doi.org/10.1016/j.cjche.2021.02.022>
40. Ausavasukhi, A., Kamposoen, C., Kengnok, O.: Adsorption characteristics of Congo red on carbonized leonardite. *J. Clean. Prod.* **134**, 506–514 (2016). <https://doi.org/10.1016/j.jclepro.2015.10.034>
41. Alavi, M.A., Morsali, A.: Ultrasonics sonochemistry syntheses and characterization of Mg(OH)<sub>2</sub> and MgO nanostructures by ultrasonic method. *Ultrason. Sonochem.* **17**(2), 441–446 (2010). <https://doi.org/10.1016/j.ultsonch.2009.08.013>
42. Lay, M., Rusli, A., Khalil, M., Ain, Z., Hamid, A., Khimi, R.: Converting dead leaf biomass into activated carbon as a potential replacement for carbon black filler in rubber composites. *Compos. Part B* **201**, 108366 (2020). <https://doi.org/10.1016/j.compositesb.2020.108366>
43. Chen, S., Wenling, Wu., Niu, Z., Kong, D., Li, W., Tang, Z., Zhang, D.: High adsorption selectivity of activated carbon and carbon molecular sieve boosting CO<sub>2</sub>/N<sub>2</sub> and CH<sub>4</sub>/N<sub>2</sub> separation. *Chin. J. Chem. Eng.* **67**, 282–297 (2024). <https://doi.org/10.1016/j.cjche.2023.10.015>

**Publisher's Note** Springer Nature remains neutral with regard to jurisdictional claims in published maps and institutional affiliations.